applied sciences

MDPI

Article

Induction Machine-Based EV Vector Control Model Using Mamdani Fuzzy Logic Controller

Humayun Salahuddin [1], Kashif Imdad [1], Muhammad Umar Chaudhry [2,*], Dmitry Nazarenko [3], Vadim Bolshev [3,4,*] and Muhammad Yasir [5]

[1] Electrical Engineering Department, HITEC University, Taxila 47080, Pakistan; humayun.15phdee002@hitecuni.edu.pk (H.S.); engr.kashif@hitecuni.edu.pk (K.I.)
[2] Department of Computer Science, MNS-University of Agriculture, Multan 59341, Pakistan
[3] Laboratory of Intelligent Agricultural Machines and Complexes, Don State Technical University, Rostov-on-Don 344000, Russia; dmnazar@mail.ru
[4] Laboratory of Power Supply and Heat Supply, Federal Scientific Agroengineering Center VIM, Moscow 109428, Russia
[5] Department of Computer Science, Faisalabad Campus, University of Engineering and Technology Lahore, Faisalabad 38000, Pakistan; muhammadyasir@uet.edu.pk
* Correspondence: umar.chaudhry@mnsuam.edu.pk (M.U.C.); vadimbolshev@gmail.com (V.B.); Tel.: +92-336-6034688 (M.U.C.); +7-499-174-8595 (V.B.)

Abstract: The substantial rise in the demand for electric vehicles (EVs) has emphasized an environment-friendly and intelligent design for speed control strategies. In this paper, a Mamdani fuzzy logic controller (MFLC) was proposed to vigorously control the speed of EVs at discrete levels. MFLC member functions (MFs) are tuned for EVs operating at three different speed modes (40, 60, and 80 km/h). The proposed speed controller operation for the speed tracking of EVs was designed and tested in MATLAB (Simulink) environment. The proposed speed controller validated a remarkable improvement in dynamic speed control compared with existing P-I, FLC, Fuzzy FOPID (ACO), Fuzzy FOPID (GA), and Fuzzy FOPID (PSO) controllers. Its stability under a user-defined drive pattern is also observed. In this proposed work, the speed controller highlights the better tracking of user-defined speed response compared to the conventional aforementioned controllers. Moreover, the speed tracking of the designed model was tested for robustness against speed transients at predefined time instants, respectively. The comparison suggests that the MFLC model removes overshoot and significantly reduces the steady-state time.

Keywords: induction machine; Mamdani fuzzy logic controller; proportional–integral; integrated gate bipolar transistor; inductance; electromagnetic torque; flux; membership function

Citation: Salahuddin, H.; Imdad, K.; Chaudhry, M.U.; Nazarenko, D.; Bolshev, V.; Yasir, M. Induction Machine-Based EV Vector Control Model Using Mamdani Fuzzy Logic Controller. *Appl. Sci.* **2022**, *12*, 4647. https://doi.org/10.3390/app12094647

Academic Editor: Jingyang Fang

Received: 8 April 2022
Accepted: 29 April 2022
Published: 5 May 2022

1. Introduction

The effects of environmental pollution on air quality demands the utilization of electric vehicle (EV) technology by introducing renewable energy sources in the place of traditional fossil fuel. In recent years, EVs have started being considered an ideal replacement for traditional vehicles due to their better operational design, efficiency, and cheaper maintenance cost [1]. The latest advancements in EVs have shown better mobility and reduced pollution in urban areas. The speed controller plays a vital role in the smooth operation of EVs, and thus researchers at industrial and academic levels have focused on the development of speed control for domestic and commercial applications. Energy management and reliable performance are key factors that need intensive analysis [2]. The EV controller should acquire desired speed with lower steady-state error and power consumption. The control system is vastly time-dependent, nonlinear, and unpredictable in terms of changing road dimensions, load parameters, and external perturbations. Therefore, the development of a speed controller that eradicates external perturbations and sustains road uncertainties with reduced control action has become the core issue to be addressed [3].

Traditional PID controllers are used in many industrial applications due to their robustness and ease-of-tuning mechanism. However, they do not perform effectively at frequently varying speeds. The emergence of artificial intelligence with PID controllers further improved PID controller performance with an effective tuning mechanism [4]. Fuzzy logic controllers (FLCs) in EV systems are capable of transforming human perception into controller design and are suitable for the management of nonlinear control parameters desired in speed control operation [5]. The precision of FLC depends on fuzzy rules developed to form a logical relation between input and output parameters.

IM multivariable parameters, nonlinear behavior, and complex mathematical models create difficulties in variable speed operations [6]. Adjustable speed controllers have been devised to handle variable speed operations [7]. The vector control technique is suitable for the variable speed drive operation of induction motor. The phasor form of indirect vector control is presented in "Figure 1". The speed sensor is used for the continuous monitoring of desired speed operation. The speed control system needs suitable arrangements to negate electrical noise. AC drive operation for variable speed requires more composite control structure leading to intelligent and smart applications. For the control of the electric drive system against abrupt changes of reference points and variations due to environmental effects, the P-I controller is suitable as a closed-loop control method. Fuzzy control is another approach that regulates the variations as per defined rules [8]. IM serves as a pillar for a wide range of speed applications ranging from small to large horsepower applications [9].

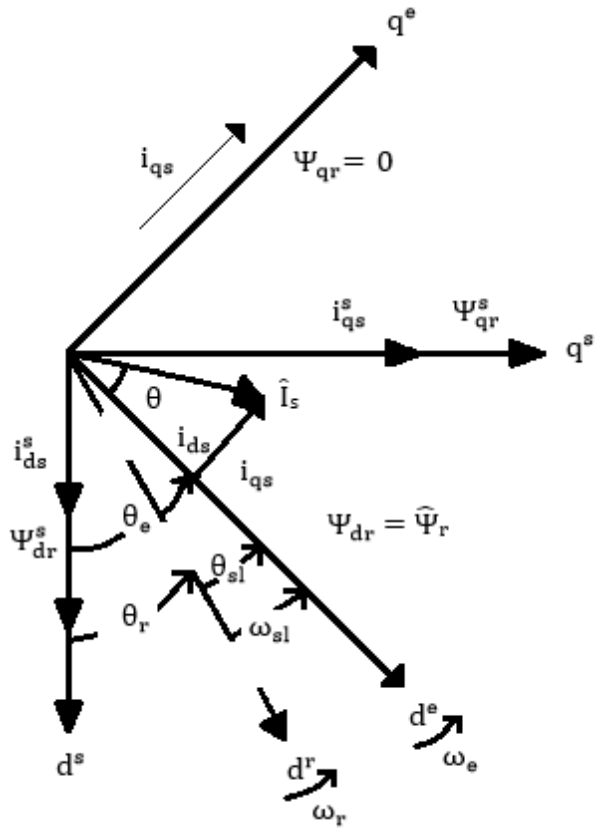

Figure 1. Phasor diagram of indirect vector control [10].

Motivation and Research Gap

The majority of the research work on the design of the fuzzy logic controllers is focused on flexibility, robustness, control blocks, computation elements, and separate control-driven systems [11]. However, the tuning of the fuzzy logic controller is achieved by input/output scaling factors on (GA, PSO, Cuckoo) optimization algorithms, respectively, [6]. ANFIS

based FOPID shows superior speed controller performance with robustness against internal and external disturbances [8,12]. Adaptive Takagi–Sugeno–Kang-fuzzy speed controller simulation presents highly robust behavior as compared to traditional control systems [13]. The simulation results of the fuzzy logic controller (FLC) based proportional–integral model waveform shows better settling time and lower peak overshoot [14]. Fuzzy regulator model performance for driverless EV enhances driving speed control in different road scenarios [15,16]. The FLC controller depicts better in terms of system stability in dynamic driving situations. Mamdani fuzzy interface system (MFIS) can be considered to model an indirect vector control system by taking datasets generated from the P-I speed controller-based indirect vector control EV model. The model was trained on MFIS to develop a logical relationship between the input and output variables. MFIS implements a superior speed controller compared to the traditional fuzzy logic control system (FLCS). It is capable of implementing the same trained model on multiple driving scenarios and abruptly adopt changes. Considering the rise in initial torque, rise time, and overshoot in EV response, a superior speed control solution using FLC at discrete speed levels to visualize smooth drive is necessary.

The objectives of the research work presented in this paper are as follows:

- Model development of IM-based indirect vector control of EV in MATLAB (Simulink) with P-I and MFIS speed controllers. Moreover, EV model performance was analyzed in three different speed modes (40, 60, 80 km/h);
- Antecedent and consequent member functions were designed in Mamdani fuzzy inference system (MFIS). The MFIS-based EV model was anticipated to improve time-domain performance indices. The capability of the controller to sustain robustness, reject external disturbance and parameter variation was verified. The controller displays improvement in speed tracking which eliminates the overshoot, and lowers the values of time-domain characteristics.
- Comparison of the proposed speed controller performance parameters with proportional–integral derivative (PID), fuzzy logic control algorithm (FLC), ant colony optimization (ACO), particle swarm optimization (PSO), and genetic algorithm (GA)-based fuzzy FOPID controllers.

The paper was arranged in the following order: Section 2 highlights the background of studies conducted for the modeling of the electric vehicle P-I and MFLC speed control operation. Section 3 gives a fuzzy MFLC speed control structure with the design information of two-dimensional membership functions and a rule base. This explains the mathematical formulation of the P-I and MFLC control model designed in MATLAB (Simulink). Both models were tested for the same operational parameters. Section 4 presents a detailed analysis of P-I and MFLC waveforms. Furthermore, the MFLC model is compared with existing FLC and fuzzy FOPID optimization algorithms for speed transitions, speed mode tracking, and uncertainties. Conclusion and future prospects are discussed in Section 5.

2. Materials and Methods

IM is reasonable in cost and strong against external disturbances. The rotor of IM tracks a rotating magnetic field that induces a voltage in rotor bars proportional to the angular speed of the magnetic field [17]. In field-oriented control, ref. [18] torque is directly controlled by armature current. The scheme for IM is the decoupling of stator dq current into i_d and i_q, where i_q generates torque and i_d creates the air gap flux. Hence, it ensures separate control for torque and flux [19]. In the case of vector control, change in the stator current proportionally relates the rotor flux to the control torque and flux independently. On the other hand, scalar control lacks accuracy [20].

2.1. Vector Control

The application of vector control for the IM drive in dynamic situations offers closed-loop speed control with robust stability. The use of IM for general purpose and industrial applications requires composite efficiency. In speed control applications, the major task of

IM is to achieve speed closely matched with reference speed irrespective of the parameter, load, or environmental uncertainties. Direct torque control governed by speed vector modulation (SVM) helps in the reduction in higher torque demand and fluctuations in flux [21]. The indirect torque control particle swarm algorithm (PSO)-tuned P-I controller offers lower ripples and a faster response time for speed and torque variations [22]. Swarm optimization highlights intermittent faults to isolate faulty components and dual gradation is used to predict the life span of faulty components [23].

The driving pattern for EV was designed in MATLAB (Simulink) to analyze vehicle speed control following a fixed route [24]. The P-I controller and fuzzy logic controller-based hybrid control of the EV model provides improvements in torque response [25]. The P-I controller mathematical form for torque generation and an error signal is shown in Equations (1) and (2) as:

$$T_e^* = K_p e(t) + K_i \int e(t)dt \quad (1)$$

$$e(t) : \omega^* - \omega \quad (2)$$

ω^*: measured speed;
ω: reference speed;
$e(t)$: error signal;
K_p: proportional gain;
K_i: integral gain;
T_e^*: generated torque.

The P-I-based speed controller in "Figure 2" lacks the rejection of load disturbance and overshoot during the tracking of the reference speed. The complex nature of the system does not permit the controller to surpass minimum permissible limits [26,27].

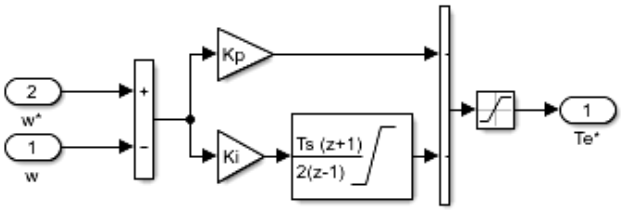

Figure 2. Simulink model P–I speed controller with torque saturator.

2.2. Fuzzy Logic Control

Fuzzy control derives its strategy as per variation in system parameters as shown in "Figure 3". The input and output variable relationship plays an important role in the derivation of rules in the fuzzy logic controller. Therefore, the careful tuning of membership functions improves system performance in diverse realizations. FLC translates a problem with ambiguous information into a well-defined solution. Logic describes the whole functionality within the domain of a mathematically described algorithm [28]. FLC implements the logic derived from the problem statement as if–then rules [29]. General-purpose nonlinear control problems are addressed with the application of fuzzy sets [30].

Electric scooter left and right gear rapid speed action is controlled by FLC. The electronic differential system sends commands to the FLC for enhanced speed action of the left and right gear [31]. The EV range is estimated by test data implemented on FLC. The FLC predicts the distance covered by EV and maintains the instantaneous consumption of power while the battery state-of-charge remains high for long-distance [32]. The comparison of the P-I controller with FLC for speed variations highlights the robust behavior of FLC. Fuzzy controller approaches reference speed parameter with better transient and steady-state response while maintaining stability [33]. The speed control error in direct torque control and indirect field-oriented control is smaller in FLC as compared with the P-I controller [34]. Hybrid electric vehicle (HEV) energy management fuzzy-control strategy

is designed for load torque demand [35,36]. EV based on FLC with vehicle speed and accumulator pressure is considered to optimize speed control operation [37]. A real-life application of the fuzzy model is observed in urban traffic control. The model highlights considerable decay in the length of the traffic queue as compared to a traditional fixed-time control approach [38].

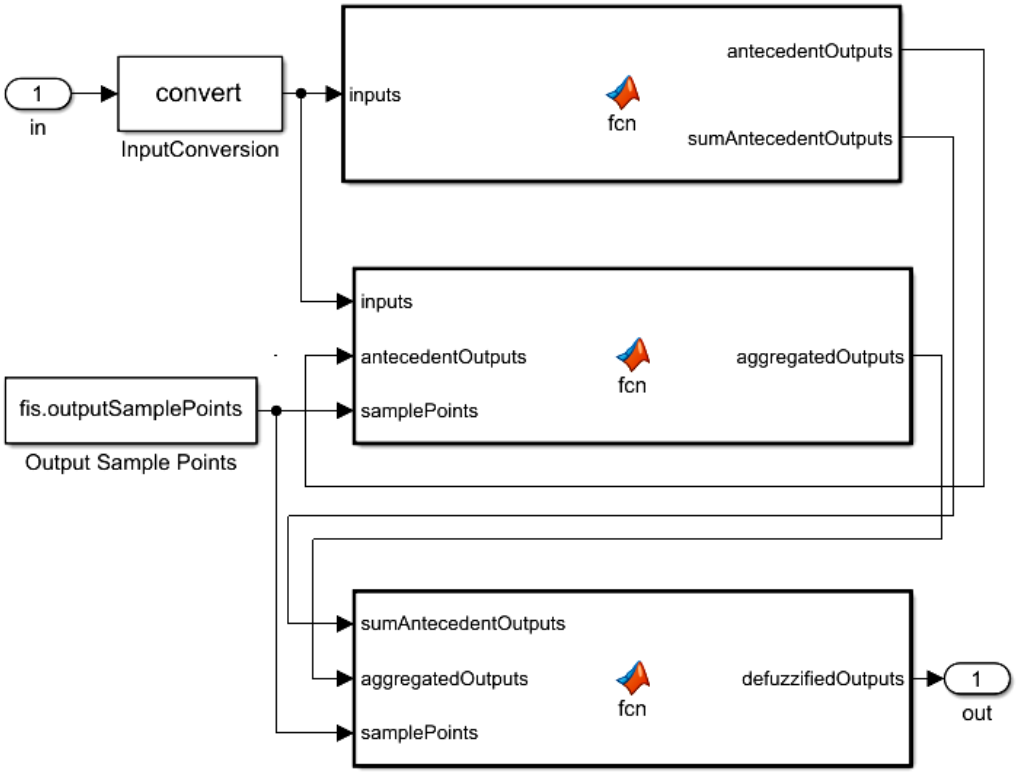

Figure 3. Simulink model flow chart of Mamdani fuzzy logic controller.

Advancements in a modern smart system with increased demand for the control of small features has created complications for orthodox methods which are not able to maintain optimum performance for complex control mechanisms. Conversely, real-life applications of the control systems are not easy to formulate correctly due to practical constraints. The exact relationship between inputs and outputs is ambiguous because of the contributions of external factors. To control such complex systems, the latest control approaches are considered to neglect external factors with good precision. A fuzzy control algorithm is one of the modern control approaches designed for complex feedback control systems. The fundamental parts of a fuzzy controller are the fuzzification interface, knowledge base, inference engine, and defuzzification interface.

Equations (1) and (2) describe the P-I controller for control action. Indirect vector control is further segregated into a P-I controller-based speed controller developed in Simulink as shown in "Figure 4". User-defined reference speed is applied to the input of the P-I speed controller. Reference speed is subtracted from the measured speed and an error signal is generated for control action. The gain of proportional and integral gains are tuned at Kp = 15 and Ki = 30. Speed controller generates torque signal. The hysteresis band current regulator compares the current signal generated from the torque command with a three-phase current measured at the input of IM. The regulator supplies six gating pulses to the IGBT inverter. "Figure 3" elaborates the flowchart of the Mamdani fuzzy logic controller (MFLC). The indirect vector control of the induction machine model developed in Simulink was elaborated in "Figure 5". The vector control block consists of a fuzzy logic controller.

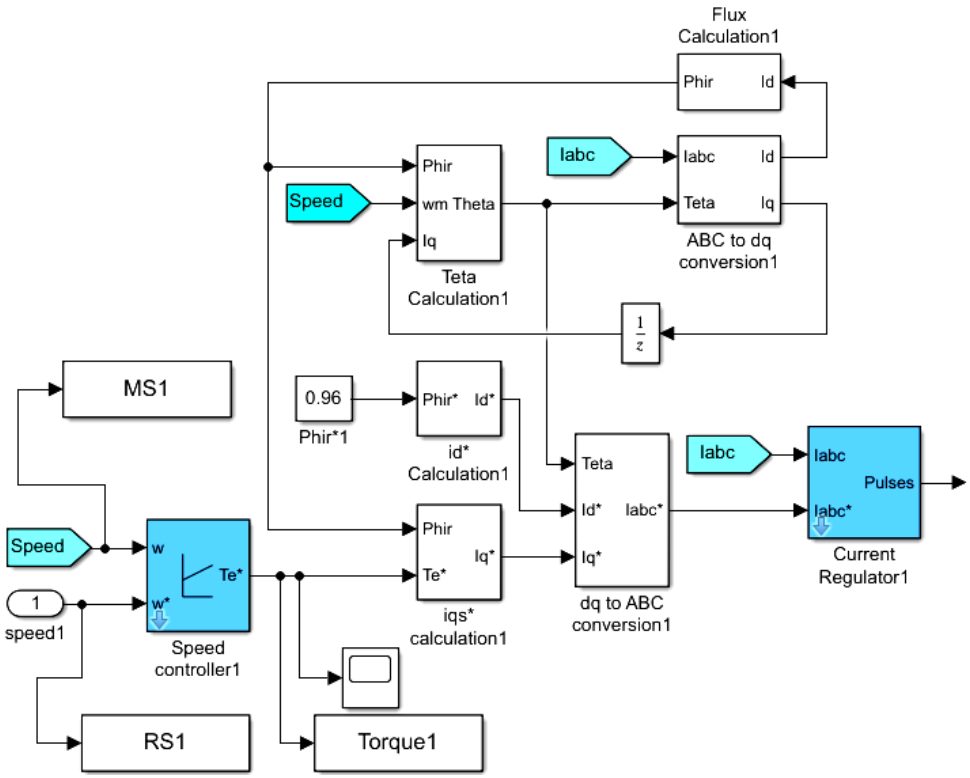

Figure 4. Simulink model of P–I control–based speed controller.

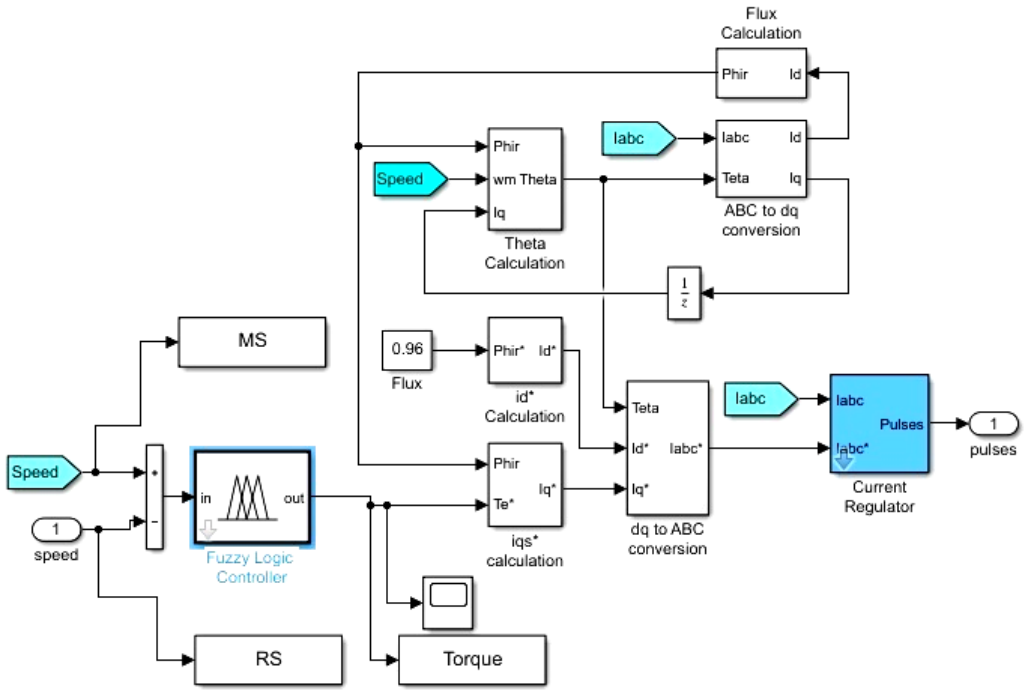

Figure 5. Simulink model of fuzzy logic controller–based vector control.

2.3. Design of P-I Speed Control Model

The P-I speed control model simulated in Matlab (Simulink) for the speed control of EV is presented in "Figure 4". P-I controller is used for controlling speed parameters. The reference speed is compared with the measured speed via a comparator block. The output of the comparator is simultaneously applied to proportional and integral controller. The gains of both controllers are adjusted as per the given error signal and the required reference

speed is finally achieved by the controller after a continuous closed-loop operation. The P-I controller generates the reference torque input and the estimated rotor flux is generated by taking a direct axis current from ABC to the dq current conversion block, whilst Equation (3) is used in the calculation of a reference quadrature axis-generated current i_{qs}^{*} required for dq to ABC current conversion; this current is compared with measured current in the current regulator block responsible for six pulses desired for optimum dc supply required for stable speed operation.

$$i_{qs}^{*} = \frac{2}{3}.\frac{2}{P}.\frac{L_r}{L_m}.\left(\frac{T_e^{*}}{|\Psi_r|_{est}}\right) \tag{3}$$

Here:

$|\Psi_r|_{est}$: Estimated rotor flux;
T_e^{*}: reference torque input generated by speed controller;
L_r: rotor inductance;
L_m: motor inductance;
L_{Ir}: rotor leakage inductance;
P: number of poles;
I_d: direct axis current;
i_{ds}^{*}: direct axis current generated;
I_q: quadrature axis current;
R_r: rotor resistance;
T_r: rotor time constant;
$|\Psi_r|^{*}$: input flux; $(phir^{*})$
ω_r: rotor speed;
ω_m: measured speed;
θ_e: theta generated;
I_a: phase a current;
I_b: phase b current;
I_c: phase c current.

Equations (4)–(9) present various parameters required for vector control action:

$$|\Psi_r|_{est} = \frac{L_m.i_d}{1 + T_r.s} \tag{4}$$

$$T_r = \frac{L_r}{R_r} \tag{5}$$

$$L_r = L_{Ir} + L_m \tag{6}$$

$$i_{ds}^{*} = \frac{|\Psi_r|^{*}}{L_m} \tag{7}$$

$$\omega_r = \frac{L_m.i_q}{T_r.|\Psi_r|^{*}} \tag{8}$$

$$\theta_e = \int (\omega_r + \omega_m) \tag{9}$$

The conversion of ABC current to dq current is presented in Equations (10) and (11) as below

$$I_d = \frac{2}{3}\left(I_a cos\theta + I_b cos\left(\theta - \frac{2}{3}\pi\right) + I_c cos\left(\theta + \frac{2}{3}\pi\right)\right) \tag{10}$$

$$I_q = -\frac{2}{3}\left(I_a sin\theta + I_b sin\left(\theta - \frac{2}{3}\pi\right) + I_c sin\left(\theta + \frac{2}{3}\pi\right)\right) \tag{11}$$

The dq current to ABC current conversion is presented in Equations (12)–(14) as

$$I_a = I_d cos\theta - I_q sin\theta \tag{12}$$

$$I_b = I_d cos\left(\theta - \frac{2}{3}\pi\right) - I_q sin\left(\theta - \frac{2}{3}\pi\right) \quad (13)$$

$$I_c = I_d cos\left(\theta + \frac{2}{3}\pi\right) - I_q sin\left(\theta + \frac{2}{3}\pi\right) \quad (14)$$

The reference three-phase current I^*_{abc} is obtained by dq to the three-phase conversion process. Here, inputs are i^*_{ds},i^*_{qs} and θ_e and the output is I^*_{abc}. The hysteresis band current regulator takes the measured current I_{abc} and current generated by dq to the three-phase converter I^*_{abc}. The output of the hysteresis band current regulator block is six gate pulses. These gate pulses are used to provide a firing angle to the IGBT switches in the inverter powered by a DC Li-ion battery. The IM was powered by an IGBT inverter. "Table 1" shows IM electrical and impedance parameters, respectively.

Table 1. Induction machine parameter values.

Symbol	Impedence Type	Value
P	rated power	50 Hp
V	voltage	460 V
R_s	stator winding resistance	87 mΩ
L_{Is}	stator leakage inductance	0.8 mH
L_m	excitation inductance	34.7 mH
R_r	rotor resistance	227 mΩ
L_{Ir}	rotor leakage inductance	0.8 mH

2.4. Design of MFLC Speed Control Model

The speed control model of the IM developed in Simulink with a fuzzy controller in place of a P-I controller is depicted in "Figure 5". However, "Figure 6" shows a general model for the indirect vector control of an induction machine developed and tested in the Simulink environment. The Vector control block consists of two controller options (PI controller and fuzzy logic controller). Reference speed and measured speed are applied at the input of the adder block. The reference speed is subtracted from the measured speed. The speed difference is connected with the input of the fuzzy logic controller block. However, the output of the fuzzy controller is the torque signal required to generate the three-phase current signal compared with measured current in the current regulator block to generate gate pulses of the IGBT inverter block. "Figure 7" presents the block diagram of the closed-loop MFLC speed controller operation.

The design of FLC intends to provide better speed control in terms of desired speed applications. FLC design maps predecessor sets with consequential sets. Initially, the FLC controller fuzzifies input vectors in Equation (15) as:

$$a = \left(a_1 :::::: ; a_n\right) \quad (15)$$

where:

a_1: first variable;
a_n: nth variable.

Here, T2U is performed by mapping input vector T towards fuzzy set U. This task is achieved by the selection of relevant membership functions (MFs) suitable to represent the variation of input parameter from a set of available MFs. The same procedure is followed to represent the output variable via the selection of the most appropriate member function from the available ones. After the selection of input and output MFs, connectivity between MFs needs to be established. If–then rules stored in the fuzzy controller database are used to relate the relationship of the input variable with the output variable. The formation of rules is based on logical operations but heavily depends on human expertise. Therefore, FLC handles system nonlinearities and the variation of parameters as input and output are mapped with the help of the rule base. The rules are designed after the careful observation

of datasets obtained by workspace named as measured speed (MS), reference speed (RS), and torque, respectively.

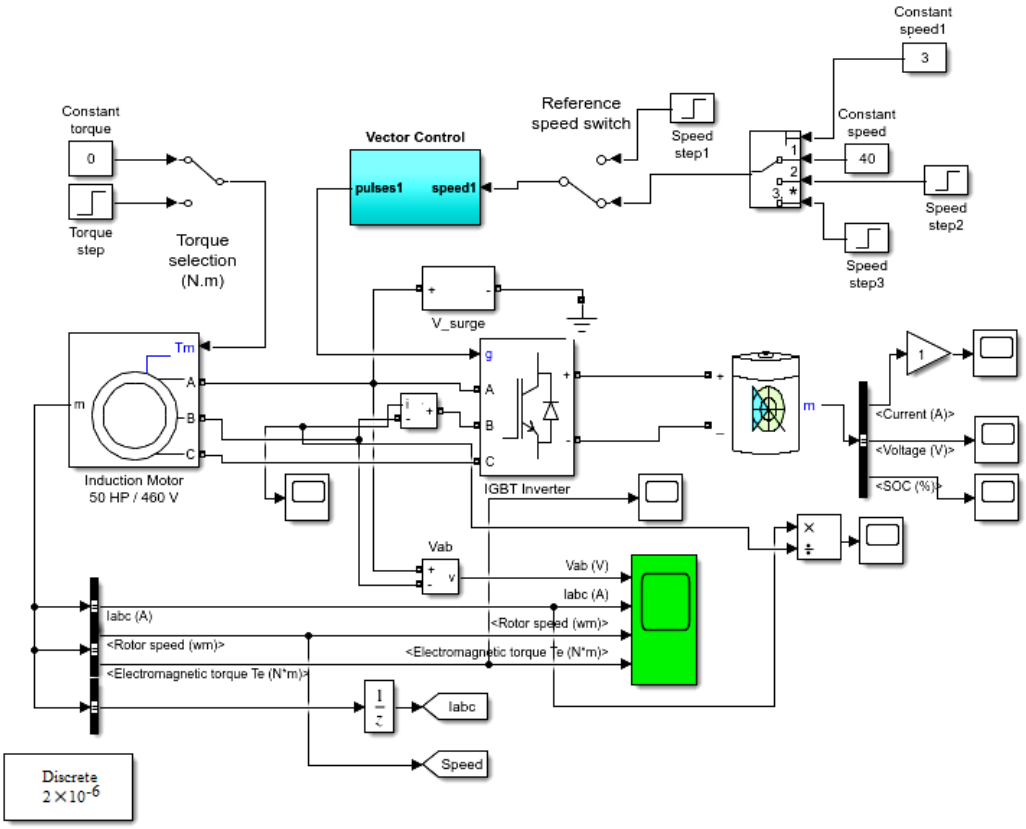

Figure 6. Simulink model of fuzzy logic controller–based vector control.

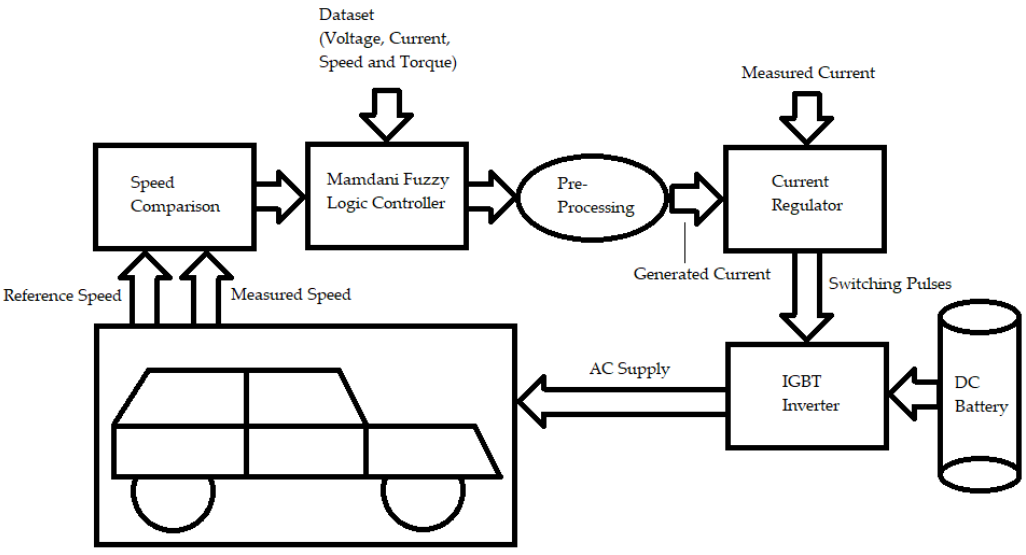

Figure 7. Block diagram of closed-loop MFLC speed control operation.

Multiple inputs contribute to the selection of the output response based on rules designed in the fuzzy controllers. The number of rules in the fuzzy controller plays an important role in the derivation of output. As each input MF is mapped with the output MF, each rule thus contributes to the output value within the range of input defined in MF. The decisions taken by the fuzzy controllers are made on binary logic. If any rule from the rule base

is true then output MF mapped with input MF will respond; otherwise, the controller traverses down towards the next rule sequentially. The MF for single input "Speed_difference" is the difference between measured speed (MS) and reference speed (RS) with a range of [−40 +5], whereas only output signal torque is in the range [−30 +330].

Seven MFs are disseminated to fill intervals for both the input and output of the fuzzy inference system (FIS). R-type trapezoidal MF is placed at the lower end of the input and output interval. L-type trapezoidal MF is placed at the higher end of the input and output interval. Moreover, the remaining interval of both input and output is filled with several triangular-shaped MFs. Input and output intervals are subdivided into seven MFs represented as (EH = extremely high; VH = very high; H = high; N = neutral; L = low; VL = very low; EL = extremely low). The seven MFs used in the model are trapezoidal (R-function, L-function) and triangular functions, respectively.

After modeling appropriate MFs (5-Triangular and 2-Trapezoidal), some rule needs to be established to individually relate input MFs with output MFs. All rules are placed on the rule base of FLC. The relationship of the input function dataset with the output function dataset is inversely proportional. This fact guides the development of rules between the respective MFs of input and output accordingly. The rule editor in Simulink provides an environment to design rules built on logical grounds. The rules are modified, added, or deleted in the rule editor. Moreover, the rule viewer provides a platform to check the distribution of MFs as per the rules established in the rule editor. The mapping curve of the input range with the output range is available in the surface viewer. Hence, the user can easily observe output value for selected input values which ultimately helps in the design of the precise and logical distribution of ranges.

The list of rules in the rule base is shown below:

1. If (Speed_difference == EL) => then(torque = EH);
2. If (Speed_difference == VL) => then (torque = VH);
3. If (Speed_difference == L) => then (torque = H);
4. If (Speed_difference == N) => then (torque = N);
5. If (Speed_difference == H) => then (torque = L);
6. If (Speed_difference == VH) => then (torque = VL);
7. If (Speed_difference == EH) => then (torque = EL).

Geometric-centroid (GC) defuzzification by Coupland and John offers a better estimation of the type-reduced centroid.

Mathematically, the center of the area (COA) is represented in Equation (16) as:

$$COA(B) \cong \frac{\sum_{i=1}^{n} y_i \mu_{\bar{B}}(y_i)}{\sum_{i=1}^{n} \mu_{\bar{B}}(y_i)} \tag{16}$$

Here:

n: number of discrete elements;
y_i: current value for ith discrete element;
$\mu_{\bar{B}}(y_i)$: relevant MF value at point y_i.

The COA provides input to the application to be controlled by FLC. In the case of a given input, the Mamdani control block fuzzifies the input and then applies the rule base to generate the output value. A rule base of seven rules is used by FLC to form the output signal. The model was tested multiple times for the correct estimation of the output from the given input signal. After adjustments in MFs and rule base, the final shape of the required response is obtained.

Triangular MF in "Figure 8" is represented by lower boundary c, upper boundary d, and a peak value m anywhere between the upper and lower boundary where the vertical value is highest. The variable "m" must satisfy the following condition $c < m < d$.

The triangular MF is presented in Equation (17) as:

$$\mu_a^x = \begin{cases} 0, & x \leq c \\ \frac{x-c}{m-c}, & c < x \leq m \\ \frac{d-x}{d-m}, & m < x < d \\ 0, & x \geq d \end{cases} \quad (17)$$

Trapezoidal MF distinct functions (R-function and L-function) are used to represent a lower and upper range of variables defined in FLC. R-functions are suitable to represent the lower limit, as shown in "Figure 9", whereas the L-function fills the upper limit area of the variable range defined in FLC. In the case of the R-function lower limit "c" and lower support limit "d" are at "$-\infty$". Moreover, an upper support limit "e" and upper limit "f" should meet the following criteria $e < f$.

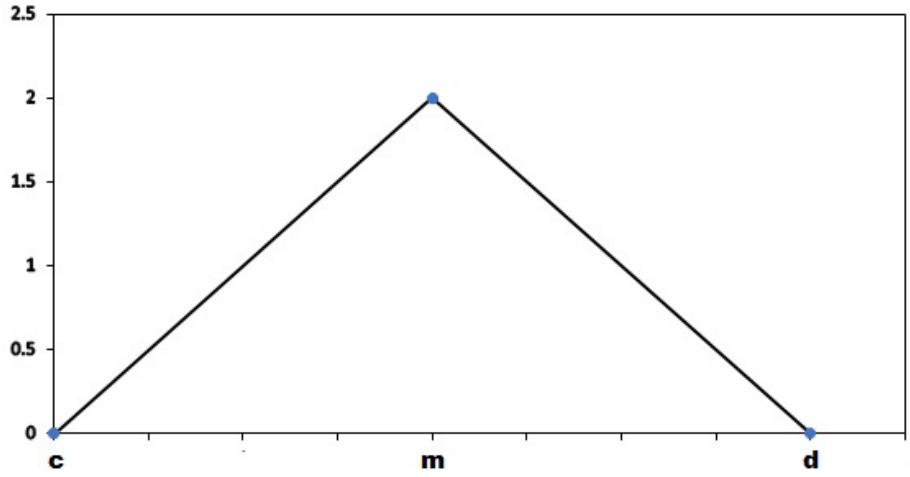

Figure 8. Triangular Member–Function.

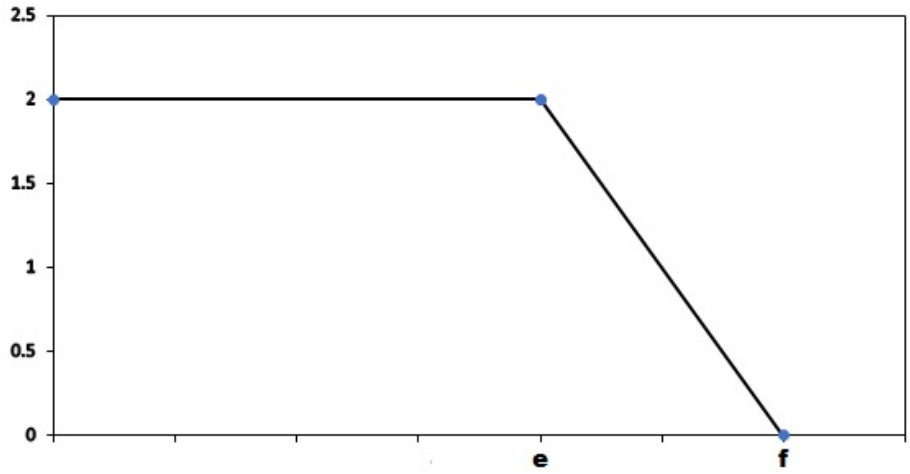

Figure 9. R–Trapezoidal Member–Function.

The trapezoidal MF (R) function is presented in Equation (18) as:

$$\mu_a^x = \begin{cases} 0, & x > e \\ \frac{f-x}{f-e}, & e \leq x \leq f \\ 1, & x < e \end{cases} \quad (18)$$

In the case of the L-function, the upper limit "f" and upper support limit "e" are at "∞" as shown in "Figure 10". Moreover, lower support limit "d" and lower limit "c" should meet the following criteria $c < d$.

The trapezoidal MF (L) function is presented in Equation (19) as:

$$\mu_a^x = \begin{cases} 0, & x < c \\ \frac{x-c}{d-c}, & c \leq x \leq d \\ 1, & x > d \end{cases} \tag{19}$$

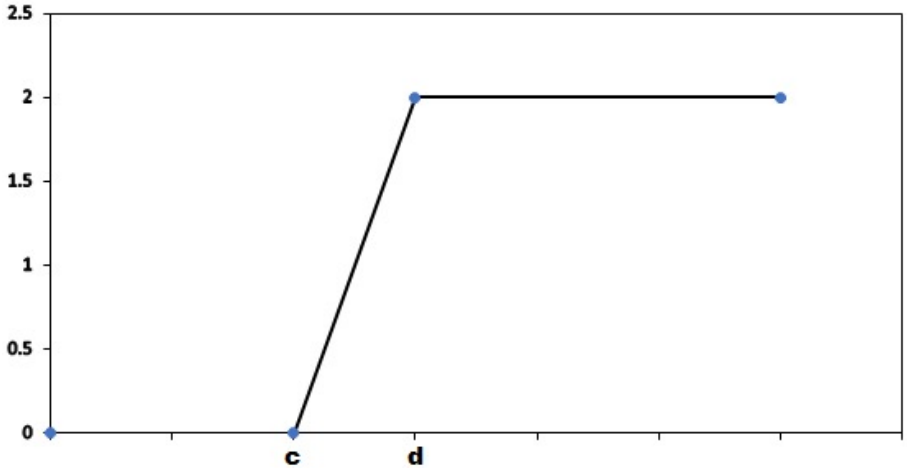

Figure 10. L–Trapezoidal Member–Function.

3. Results

P-I and MFLC EV speed control models shown in "Figures 4–6" are designed using the MATLAB (Simulink) environment. This section illustrates the dominance of the fuzzy MFLC controller over the P-I controller, fuzzy FOPID (ACO) controller, fuzzy FOPID (GA) controller, and fuzzy FOPID (PSO) controller through the evaluation of EV's speed tracking operation. The parameters of the fuzzy MFLC speed controller are shown in "Figures 8–11".

The input variable of FLC is "Speed_difference", whereas the output parameter is "Torque". The range of input and output is matched by taking the dataset from the P-I speed controller model. Member functions (triangular and trapezoidal) are presented in Figures 8–10. The fuzzy logic designer (FLD) in Figure 11a provides an overview of the input and output limitations. The Mamdani block holds the rules developed to map input MFs with output MFs based on logical conditions. Furthermore, the defuzzification method "centroid" is selected for the desired fuzzy logic control operation. In the membership function editor (MFE), "Speed_difference" MFs are arranged after matching with "Torque" MFs, as shown in Figure 11b,c, respectively. The range for the input variable and output variable is visible in MFE. Once the rules are established, the rule viewer (RV) in Figure 11d provides a visual presentation of the output variable value as per selected input. This feature is beneficial to check for any mistakes in rules derived from the RE interface of FLC. The surface view (SV) in "Figure 11e" presents a graphical picture of the relationship between the input and output variables, respectively.

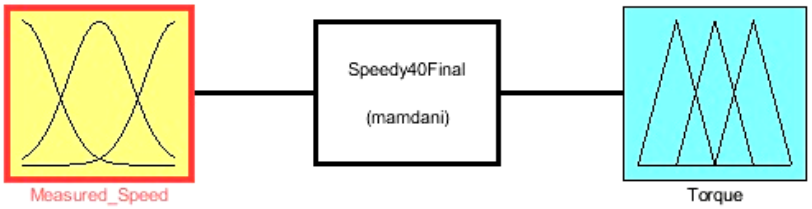

(**a**)

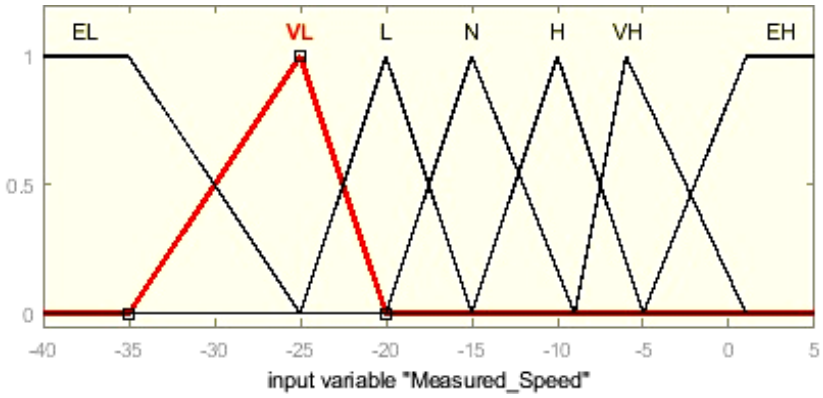

(**b**)

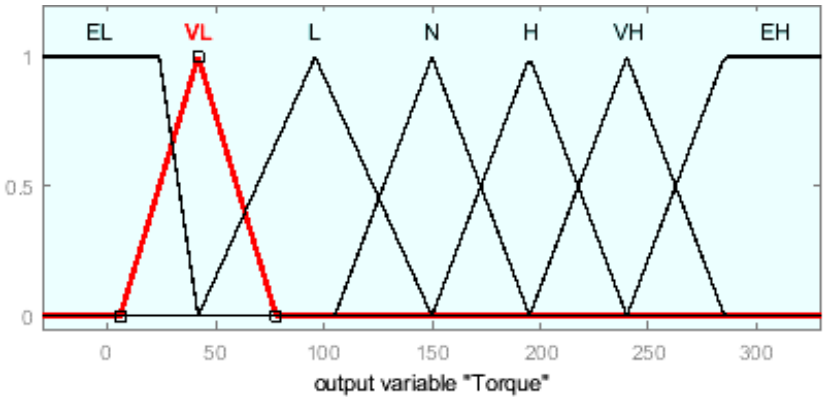

(**c**)

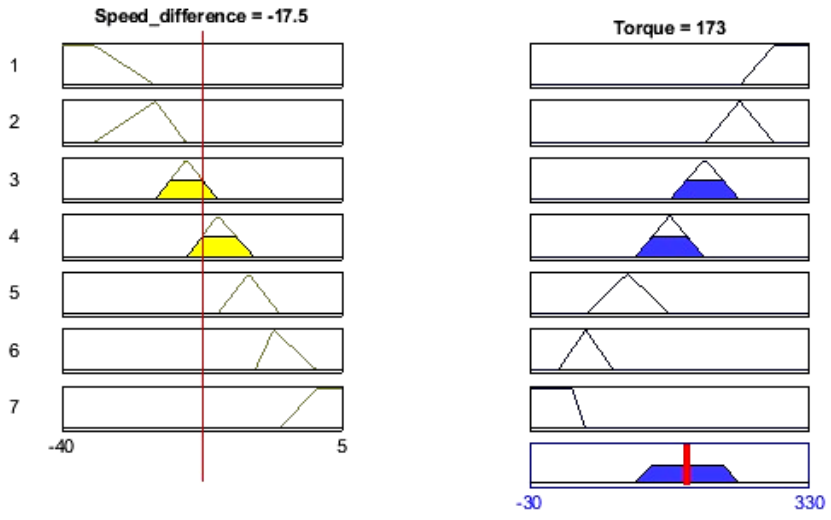

(**d**)

Figure 11. *Cont.*

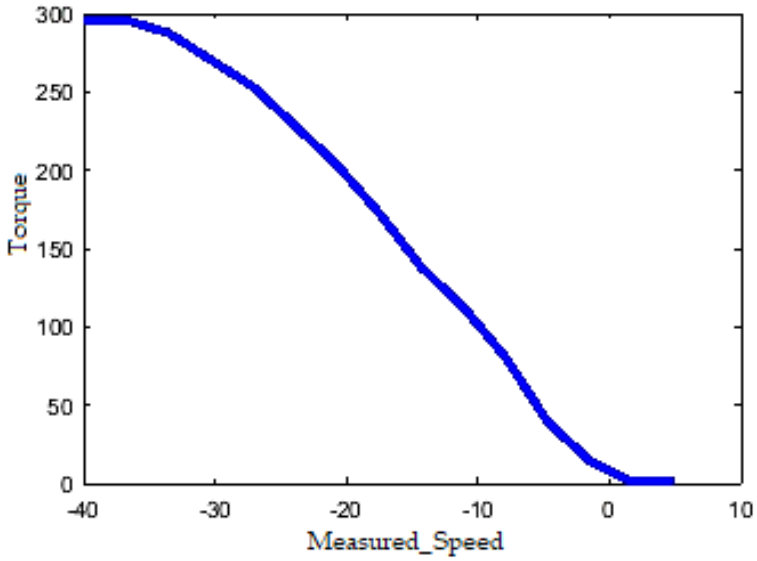

(**e**)

Figure 11. Mamdani fuzzy logic controller Simulink environment: (**a**) fuzzy logic designer; (**b**) input membership function; (**c**) output membership function; (**d**) rule viewer; and (**e**) output surface of MFLC.

4. Discussion

The P-I speed controller and proposed fuzzy MFLC controller's performance to track reference speed is compared in "Figures 12 and 13". This shows variation in the three-phase current, rotor speed, and torque from rest to small, medium, and high-speed transitions for the time duration (8 s). First and foremost, a speed transition of 40 km/h was applied at a time of 0 s in both figures. Following, the second transition of 60 km/h was applied at times of 2.0 s and 1.0 s, respectively. A final speed transition of 80 km/h was applied at times of 4.0 s and 2.0 s, respectively. As it can be concluded that while the P-I speed controller produces higher control effort and steady-state error, the fuzzy MFLC generates a lower control effort and steady-state error, which enriches its performance.

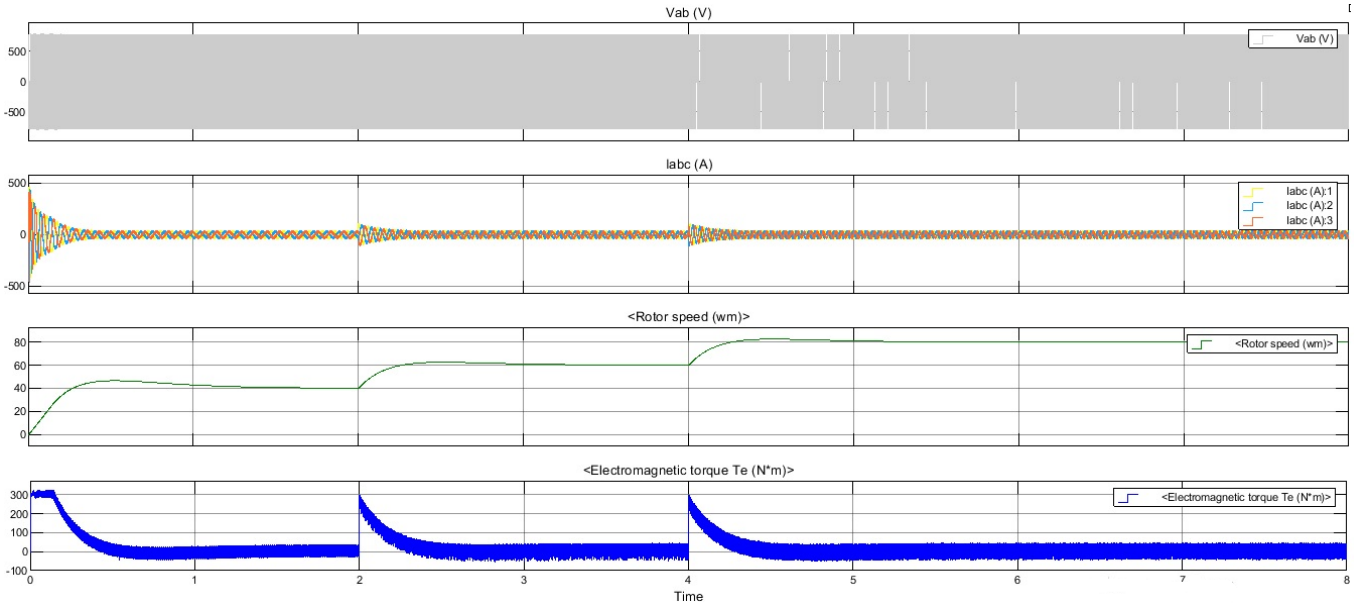

Figure 12. Overall P–I speed controller performance comparison (0–40, 40–60, 60–80) representing the induction machine application in the EV model for different speed modes to compare its effects on torque, current, and voltage, respectively.

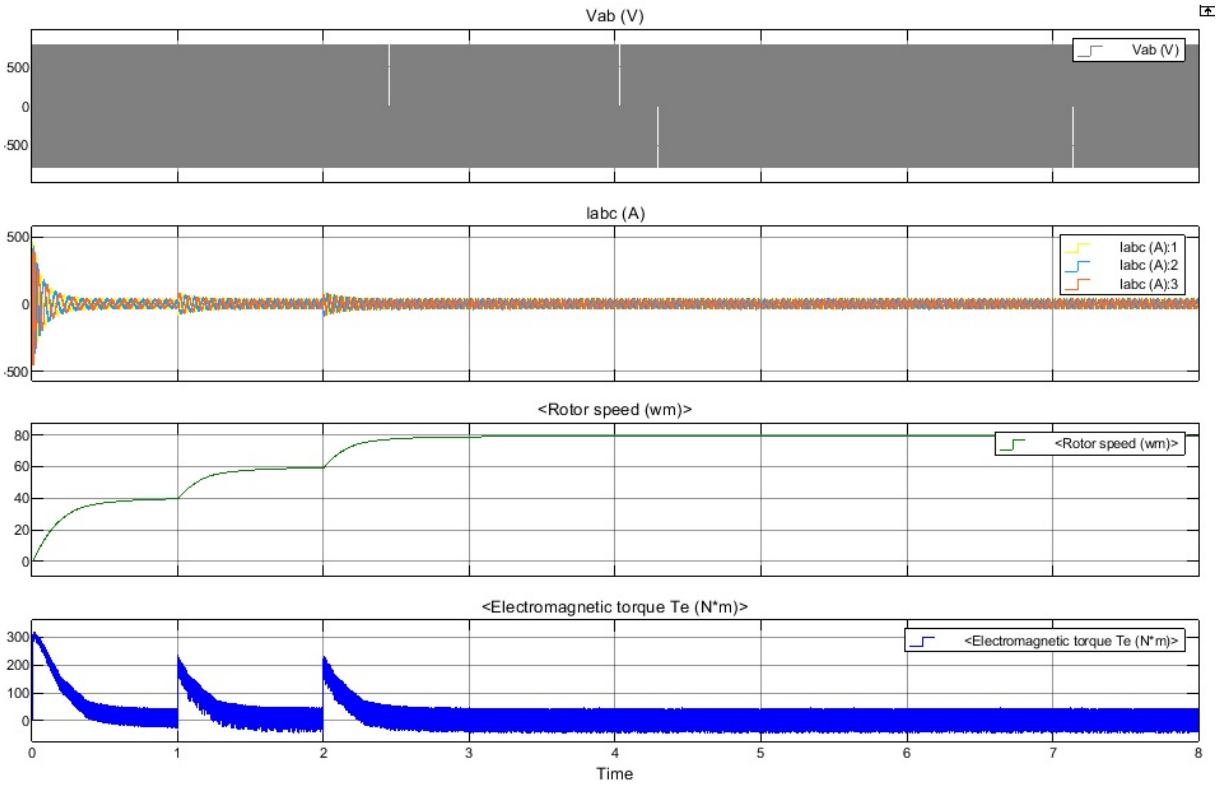

Figure 13. Overall MFLC speed controller performance comparison (0–40, 40–60, 60–80) representing the induction machine application in the EV model for different speed modes, respectively, to compare its effects on torque, current, and voltage, respectively.

Tables 2–4 summarize the performance parameters of P-I and the proposed fuzzy MFLC speed controller for predefined speed transitions. Time-domain factors such as the rise time, settling time peak time, and overshoot are compared for both controllers. In terms of reference speed tracking, both controllers track the reference speed. However, after critically watching the pattern of waveforms, the proposed Mamdani-FLC controller was much better than the P-I controller with higher accuracy, zero overshoot, and negligible steady-state error. The response time of the P-I controller and Mamdani-FLC for a speed transition 40 km/h was: 1.6 s and 0.7 s; for a speed transition of 60 km/h was: 1.3 s and 0.7 s; and for a speed transition of 80 km/h was: 1.2 s and 1.1 s, respectively. The total response time taken by the P-I speed controller was 4.1 s as compared to Mamdani-FLC which is 2.5 s. Hence, a fuzzy MFLC controller requires a lesser settling time compared to a P-I controller. The overshoot for the P-I controller is observed as 14%, 7%, and 5% for small, medium, and large speed transitions. The Mamdani-FLC completely removes the overshoot which indicates the suitability of a later model for speed control application in EVs.

Table 2. Performance comparison between P-I controller and Mamdani fuzzy logic controller (low-speed transition).

Speed Controller Type	Rise Time (T_r)	Settling Time (T_s)	Peak Time	Overshoot Percentage
P-I controller	0.25 s	1.6 s	0.55 s	14
Mamdani FLC	0.5 s	0.7 s	0.7 s	0

s = second.

Table 3. Performance comparison between P-I controller and Mamdani fuzzy logic controller (medium-speed transition).

Speed Controller Type	Rise Time (T_r)	Settling Time (T_s)	Peak Time	Overshoot Percentage
P-I controller	0.2 s	1.3 s	0.5 s	7
Mamdani FLC	0.5 s	0.7 s	0.7 s	0

s = second.

Table 4. Performance comparison between P-I controller and Mamdani fuzzy logic controller (high-speed transition).

Speed Controller Type	Rise Time (T_r)	Settling Time (T_s)	Peak Time	Overshoot Percentage
P-I controller	0.18 s	1.2 s	0.45 s	6
Mamdani FLC	0.55 s	1.1 s	1.1 s	0

s = second.

Figure 13 displays the superior performance of the fuzzy MFLC controller for a speed transition of 40 km/h. The waveform shows a convergence of speed as per the agreed speed transition. Moreover, it reaches a step-change in speed within minimum time and tracks the reference speed via the fuzzy closed-loop feedback control system. This further indicates the speed controller performance for a speed transition of 60 km/h. Finally, a speed transition of 80 km/h was observed for the high-speed operation of EV. The fuzzy MFLC model was tested for multiple speed scenarios for understanding driving requirements. From rest to motion torque of IM reaches the highest value of 300 N.m initially but it drops to the minimum value as reference speed is achieved. The three-phase current follows the torque trend. It initially reaches maximum value against torque 300 N.m then follows the decreasing trend and reaches its minimum value as the torque reaches its lowest value. The torque and current levels of Mamdani-FLC are smaller as compared to the P-I controller response as shown in "Figures 12 and 13" respectively. The result indicates that the P-I controller cannot effectively track the desired speed of the fuzzy MFLC controller. This shows the efficient handling of EV parameters as energy can be saved and effectively supplied for a longer duration. The robustness is observed in fuzzy MFLC controllers by introducing disturbance (transition speed) as a step function. The fuzzy controller can swiftly reach the desired value after externally introducing disturbance. An efficient speed controller must reject the disturbance within minimum time and deviation from desired speed.

The proposed fuzzy MFLC speed controller tracking operation was compared with P-I, FLC, fuzzy FOPID (ACO), fuzzy FOPID (GA), and fuzzy FOPID (PSO) controllers. The operational characteristics of all controllers are compared at the same speed of 40 km/h. Table 5 gives the time-domain parameters of the EV model using the aforementioned controllers. It is observed from the results that the fuzzy MFLC controller is superior to the aforementioned controllers in terms of settling time and overshoot percentage. The increase in increase time provides a smooth curve towards the desired speed without overshoot. Furthermore, the fuzzy MFLC speed controller is taking a step-change in speed level as compared to the ramp curve applied for the aforementioned controllers which guarantee the reliable performance of a speed controller under dynamic driving situations.

Irrespective of certain advantages of the speed controller model, it has some design limitations: transforming the rule base for Mamdani fuzzy logic controller (MFLC) to meet predefined speed transitions takes time as it demands prerequisite experience and expertise. The model is trained for three speed modes 40, 60, and 80. The model works on fixed speed and achieves the desired speed based on pre-defined speed mode. The model is not valid for driverless EVs.

Table 5. Performance comparison between P-I controller and Mamdani fuzzy logic controller with fuzzy FOPID speed controllers (small speed transition).

Speed Controller Type	Rise Time (T_r)	Settling Time (T_s)	Peak Time	Overshoot Percentage
P-I controller	0.25 s	1.6 s	0.55 s	14
Mamdani FLC	0.5 s	0.7 s	0.7 s	0
FLC [7]	0.547 s	1.868 s	1.868 s	0.489
Fuzzy FOPID ACO [6]	0.081 s	0.75 s	0.75 s	0.505
Fuzzy FOPID GA [6]	0.19 s	1.4 s	1.4 s	0.8
Fuzzy FOPID PSO [6]	0.12 s	1.2 s	1.2 s	0.72

s = second.

5. Conclusions

This study presented an indirect vector control EV model implemented with salient features of Mamdani FLC. The EV model operates at three discrete speed modes (40, 60 and 80 km/h), respectively. A comprehensive evaluation of MFLC is performed concerning the P-I controller, FLC, fuzzy FOPID ACO, fuzzy FOPID GA, and fuzzy Fopid PSO. The proposed speed controller offers reckless speed tracking with a rise time of 0.5 s and a settling time of 0.7 s. Moreover, it performs remarkable speed tracking with zero overshoot. The results generated from the simulation revealed that the proposed speed controller could brilliantly handle abrupt variation in parameters, external disturbance, and uncertainties. The drop in torque, 3-phase current, rise time, and the removal of overshoot prove the efficient implementation of the MFLC EV model for handling diverse real-time road scenarios. This research work provides valuable insight for future state-of-the-art machine learning algorithms as well as IOT can be integrated to meet the desired speed in driverless EVs.

Author Contributions: Conceptualization, H.S. and K.I.; methodology, H.S., K.I. and M.U.C.; software, D.N. and V.B.; validation, H.S., M.U.C. and D.N.; formal analysis, H.S. and K.I.; investigation, D.N., M.Y. and V.B.; resources, K.I., M.Y. and M.U.C.; data curation, K.I. and M.Y.; writing—original draft preparation, H.S. and K.I.; writing—review and editing, M.U.C., V.B. and H.S.; visualization, D.N. and M.Y.; supervision, K.I., D.N. and V.B.; project administration, M.U.C.; funding acquisition, D.N. and V.B. All authors have read and agreed to the published version of the manuscript.

Funding: This research was funded by RF state assignment No. 075-03-2021-019/5 (Development of a set of technological solutions for creating a universal domestic platform for an electric vehicle with a high energy density battery, an energy efficient drive with high torque and electric energy regeneration function).

Institutional Review Board Statement: Not applicable.

Informed Consent Statement: Not applicable.

Data Availability Statement: Not applicable.

Conflicts of Interest: The authors declare no conflict of interest.

References

1. Salah, W.A.; Albreem, M.A.; Alsayid, B.; Zneid, B.A.; Alkhasawneh, M.; Al-Mofleh, A.; Al-Aish, A.A. Electric vehicle technology impacts on energy. *Int. J. Power Electron. Drive Syst.* **2019**, *10*, 1. [CrossRef]
2. Arfeen, Z.A.; Khairuddin, A.B.; Munir, A.; Azam, M.K.; Faisal, M.; Arif, M.S.B. En route of electric vehicles with the vehicle to grid technique in distribution networks: Status and technological review. *Energy Storage* **2020**, *2*, e115. [CrossRef]
3. Arfeen, Z.A.; Abdullah, M.P.; Sheikh, U.U.; Azam, M.K.; Sule, A.H.; Fizza, G.; Khan, M.A. Novel Supervisory Management Scheme of Hybrid Sun Empowered Grid-Assisted Microgrid for Rapid Electric Vehicles Charging Area. *Appl. Sci.* **2021**, *11*, 9118. [CrossRef]
4. Lee, J.H.; Chakraborty, D.; Hardman, S.J.; Tal, G. Exploring electric vehicle charging patterns: Mixed usage of charging infrastructure. *Transp. Res. Part Transp. Environ.* **2020**, *79*, 102249. [CrossRef]
5. Lee, Z.J.; Lee, G.; Lee, T.; Jin, C.; Lee, R.; Low, Z.; Low, S.H. Adaptive charging networks: A framework for smart electric vehicle charging. *IEEE Trans. Smart Grid* **2021**, *12*, 4339–4350. [CrossRef]

6. George, M.A.; Kamat, D.V.; Kurian, C.P. Electronically Tunable ACO Based Fuzzy FOPID Controller for Effective Speed Control of Electric Vehicle. *IEEE Access* **2021**, *9*, 73392–73412. [CrossRef]
7. Kassem, R.; Sayed, K.; Kassem, A.; Mostafa, R. Power optimisation scheme of induction motor using FLC for electric vehicle. *IET Electr. Syst. Transp.* **2020**, *10*, 301–309. [CrossRef]
8. Joshi, G.; Pius, P. ANFIS controller for vector control of three phase induction motor. *Indones. J. Electr. Eng. Comput. Sci. (IJEECS)* **2020**, *19*, 1177–1185. [CrossRef]
9. Buticchi, G.; Gerada, D.; Alberti, L.; Galea, M.; Wheeler, P.; Bozhko, S.; Gerada, C. Challenges of the optimization of a high-speed induction machine for naval applications. *Energies* **2019**, *12*, 2431. [CrossRef]
10. Osorio, J.; Ponce, P.; Molina, A. Electric Vehicle Powertrain Control with Fuzzy Indirect Vector Control. In Proceedings of the 2012 11th Mexican International Conference on Artificial Intelligence, San Luis Potos, Mexico, 27 October–4 November 2012; pp. 122–127.
11. Monicka, J.G.; Sekhar, N.G.; Kumar, K.R. Performance evaluation of membership functions on fuzzy logic controlled ac voltage controller for speed control of induction motor drive. *Int. J. Comput. Appl.* **2011**, *13*, 8–12.
12. George, M.A.; Kamat, D.V.; Kurian, C.P. Electric vehicle speed tracking control using ANFIS based fractional order PID controller. *J. King Saud Univ.-Eng. Sci.* **2022**. [CrossRef]
13. Wang, S.Y.; Tseng, C.L.; Chiu, C.J. Design of a novel adaptive TSK-fuzzy speed controller for use in direct torque control induction motor drives. *Appl. Soft Comput.* **2015**, *31*, 396–404. [CrossRef]
14. Sayed, K.; Gabbar, H.A. Electric vehicle to power grid integration using three-phase three-level AC/DC converter and PI-fuzzy controller. *Energies* **2016**, *9*, 532. [CrossRef]
15. Birajdar, M.R.; Patait, T.B.; Sayyad, A.R.; Jangam, P.S.; Bhosle, S.S.; Malgave, A.A. Electrical vehicle speed control by AI technique. *Asian J. Converg. Technol. (AJCT)* **2021**, *7*, 25–28. [CrossRef]
16. Sahbani, A.; Mahersia, H. Advanced Driving Assistance System for an Electric Vehicle Based on Deep Learning. In *New Perspectives on Electric Vehicles*; IntechOpen: London, UK, 2021.
17. Kastha, D.; Bose, B.K. Investigation of fault modes of voltage-fed inverter system for induction motor drive. *IEEE Trans. Ind. Appl.* **1994**, *30*, 1028–1038. [CrossRef]
18. Krishnan, R.; Bharadwaj, A.S. A review of parameter sensitivity and adaptation in indirect vector controlled induction motor drive systems. *IEEE Trans. Power Electron.* **1991**, *6*, 695–703. [CrossRef]
19. Mishra, A.; Choudhary, P. Speed control of an induction motor by using indirect vector control method. *IEEE Trans. Power Electron.* **2012**, *2*, 144–150.
20. Liu, L.; Du, X.; Shen, S. Indirect field-oriented torque control of induction motor considering magnetic saturation effect: Error analysis. *IET Electr. Power Appl.* **2017**, *11*, 1105–1113. [CrossRef]
21. Ammar, A.; Benakcha, A.; Bourek, A. Closed loop torque SVM-DTC based on robust super twisting speed controller for induction motor drive with efficiency optimization. *Int. J. Hydrogen Energy* **2017**, *42*, 17940–17952. [CrossRef]
22. Humod, A.T.; Abdullah, M.N.; Faris, F.H. A comparative study between vector control and direct torque control of induction motor using optimal controller. *Int. J. Sci. Eng. Res.* **2016**, *7*, 1362–1371.
23. Xiao, C.; Yu, M.; Wang, H.; Zhang, B.; Wang, D. Prognosis of Electric Scooter With Intermittent Faults: Dual Degradation Processes Approach. *IEEE Trans. Veh. Technol.* **2022**, *71*, 1411–1425. [CrossRef]
24. Anida, I.N.; Salisa, A.R. Driving cycle development for Kuala Terengganu city using k-means method. *Int. J. Electr. Comput. Eng.* **2019**, *9*, 1780. [CrossRef]
25. Deshpande, G.V.; Sankeshwari, S.S. Speed control of induction motors using hybrid pi plus fuzzy controller. *Int. J. Adv. Eng. Technol.* **2013**, *6*, 2253.
26. Jain, J.K.; Ghosh, S.; Maity, S. Concurrent PI controller design for indirect vector controlled induction motor. *Asian J. Control* **2020**, *22*, 130–142. [CrossRef]
27. Emil Hasan, A.; Hassan, H.; Bugis, I. Variable Speed Vector Control for Induction Motor of Electric Vehicle. *Appl. Mech. Mater.* **2015**, *699*, 759–764. [CrossRef]
28. Ma, K.; Wang, Z.; Liu, H.; Yu, H.; Wei, C. Numerical investigation on fuzzy logic control energy management strategy of parallel hybrid electric vehicle. *Energy Procedia* **2019**, *158*, 2643–2648. [CrossRef]
29. Sharma, K.D.; Ayyub, M.; Saroha, S.; Faras, A. Advanced controllers using fuzzy logic controller (FLC) for performance improvement. *Int. Electr. Eng. J. (IEEJ)* **2014**, *5*, 1452–1458.
30. Ahmad, N.S. Robust H∞-Fuzzy Logic Control for Enhanced Tracking Performance of a Wheeled Mobile Robot in the Presence of Uncertain Nonlinear Perturbations. *Sensors* **2020**, *20*, 3673. [CrossRef]
31. Hichem, C.; Nasri, A.; Kayisli, K. Fuzzy Logic Speed Control for Three-Wheel Electric Scooter. *Int. J. Renew. Energy Res. (IJRER)* **2019**, *9*, 1443–1450.
32. Çeven, S.; Albayrak, A.; Bayır, R. Real-time range estimation in electric vehicles using fuzzy logic classifier. *Comput. Electr. Eng.* **2020**, *83*, 106577. [CrossRef]
33. Tir, Z.; Soufi, Y.; Hashemnia, M.N.; Malik, O.P.; Marouani, K. Fuzzy logic field oriented control of double star induction motor drive. *Electr. Eng.* **2017**, *99*, 495–503. [CrossRef]
34. Aktas, M.; Awaili, K.; Ehsani, M.; Arisoy, A. Direct torque control versus indirect field-oriented control of induction motors for electric vehicle applications. *Eng. Sci. Technol. Int. J.* **2020**, *23*, 1134–1143. [CrossRef]

35. Singh, K.V.; Bansal, H.O.; Singh, D. Feed-forward modeling and real-time implementation of an intelligent fuzzy logic-based energy management strategy in a series–parallel hybrid electric vehicle to improve fuel economy. *Electr. Eng.* **2020**, *102*, 967–987. [CrossRef]
36. Srikanth, R.; Venkatesan, M.; Subba Rao, M. Design and performance evaluation of PID, Fuzzy logic and ANN controllers based MPPTs for hybrid electric vehicle applications. *Int. J. Ambient. Energy* **2020**, 1–15. [CrossRef]
37. Yang, J.; Zhang, T.; Hong, J.; Zhang, H.; Zhao, Q.; Meng, Z. Research on Driving Control Strategy and Fuzzy Logic Optimization of a Novel Mechatronics-Electro-Hydraulic Power Coupling Electric Vehicle. *Energy* **2021**, *233*, 121221. [CrossRef]
38. Jafari, S.; Shahbazi, Z.; Byun, Y.C. Traffic Control Prediction Design Based on Fuzzy Logic and Lyapunov Approaches to Improve the Performance of Road Intersection. *Processes* **2021**, *9*, 2205. [CrossRef]